Journal of the Geological Society, London, Vol. **161**, 2004, pp. 93–101. Printed in Great Britain.

Structural and thermal history of poly-orogenic basement: U–Pb geochronology of granitoid rocks in the southern Menderes Massif, Western Turkey

KLAUS GESSNER[1], ALAN S. COLLINS[2], UWE RING[3] & TALIP GÜNGÖR[4]

[1]*Computational Geoscience, CSIRO Exploration and Mining, Australian Resources Research Centre, PO Box 1130, Bentley, W.A. 6102, Australia (e-mail: Klaus.Gessner@csiro.au)*

[2]*Tectonics Special Research Centre, Department of Applied Geology, Curtin University of Technology, GPO Box U1987, Perth, W.A. 6845, Australia*

[3]*Institut für Geowissenschaften, Becherweg 21, Johannes Gutenberg-Universität, 55099 Mainz, Germany*

[4]*Jeoloji Mühendisliği Bölümü, Dokuz Eylül Üniversitesi, 35100 Bornova (İzmir), Turkey*

Abstract: Ion microprobe U–Pb dating of granitoid rocks from key structural outcrops of the Menderes Massif in western Turkey provides an important constraint to the thermal and deformational history of a structurally complex metamorphic belt within the Alpine chain. Crystallization ages of two granite protoliths, derived from the weighted means of rim ages and the ages of homogeneous prismatic zircon grains, are 541 ± 14 Ma and 566 ± 9 Ma, whereas the cores of zoned pyramidal and short-prismatic zircon grains range from Palaeoproterozoic to Neoproterozoic in age. These ages indicate that amphibolite- to granulite-facies metamorphic rocks in much of the Menderes Massif were deformed, metamorphosed and intruded during the Pan-African Orogeny, and neither crystallized nor remelted during an Alpine event. Structural and metamorphic evidence for Alpine convergence in Pan-African basement rocks is limited to greenschist-facies top-to-the-south shear zones, which occur on a regional scale across a number of tectonic units.

Keywords: $^{238}U/^{206}Pb$, Alpine Orogeny, Pan-African Orogeny, Turkey, polyphase processes, tectonics.

Detailed structural analysis coupled with high spatial precision geochronology, such as secondary ionization mass spectroscopy (SIMS) using the sensitive high-mass resolution ion microprobe (SHRIMP), has the potential to resolve structural and thermal history of poly-orogenic terranes (e.g. Nutman *et al*. 1989; Kinny & Friend 1997). This is particularly true for geological terranes where events occurred widely separate in time, as in the case of the Menderes Massif in western Turkey (Fig. 1), where Neoproterozoic and Tertiary orogenic events are superposed.

The Menderes Massif (Paréjas 1940) and the overlying Lycian Allochthon (de Graciansky 1972; Okay 1989; Robertson *et al*. 1996; Collins & Robertson 1997, 1998, 1999, 2003) constitute the western Turkish part of the Anatolide belt (Fig. 1a), which formed as a result of Alpine collision tectonics in the early Tertiary (Şengör & Yilmaz 1981; Şengör *et al*. 1984; Ring *et al*. 1999; Gessner *et al*. 2001*c*) and has been overprinted by continental extension tectonics since the Miocene (e.g. Şengör 1987; Seyitoğlu *et al*. 1992; Hetzel *et al*. 1995; Gessner *et al*. 2001*b*; Lips *et al*. 2001). However, a number of geodynamically important controversies exist that hinder efforts at creating a consensus on the region's evolution. This study aims to resolve the controversy as to whether the age of the granitoid magmatism, and the amphibolite-facies deformation fabrics and associated kinematic indicators, are of Neoproterozoic or of Tertiary age (Bozkurt *et al*. 1993; Gessner *et al*. 2001*a*, 2001*c*; Lips *et al*. 2001). The age of magmatism and deformation are of key importance for an understanding of the structural and thermal history of the Anatolide belt and the geodynamics of this part of the Alpine orogenic system. Because of the good exposure of a crustal section normal to foliation and tectonic boundaries, the southern margin of the the Çine submassif (Fig. 1) has long been regarded as a key region to understand the tectonic evolution of the Menderes Massif, and has been the subject of a number of detailed structural, metamorphic and geochronological studies (e.g. Ashworth & Evirgen 1984; Bozkurt *et al*. 1993; Hetzel & Reischmann 1996; Whitney & Bozkurt 2002; Régnier *et al*. 2003). For this study *in situ* SIMS analyses were carried out to determine the U and Pb isotope compositions of different domains within zircon grains. The data are used to determine the crystallization age of crosscutting granites in two key structural outcrops in the southern part of the Çine submassif. It will be shown that neither zircon growth nor isotopic resetting has occurred since late Neoproterozoic to Cambrian times, which effectively rules out the occurrence of remelting, high-grade metamorphism and associated deformation fabrics during the Tertiary Alpine Orogeny.

Geodynamic models and their structural expression

Most geodynamic hypotheses of the Anatolide belt in western Turkey involve the southeastward transport of an ophiolite (Lycian Peridotite Thrust Sheet) and an underlying imbricated passive margin succession (Lycian Thrust Sheets) from NW to SE, over the site of the present Menderes Massif (Collins & Robertson 1997, 1998, 1999, 2003; Gessner *et al*. 2001*a*, 2001*c*). The combined transported units (the Lycian Allochthon) were thrust southeastward in stages from the latest Cretaceous to Miocene times (Collins & Robertson 1998). There is little consensus, however, on the structural and thermal evolution of the complex imbrication of poly-metamorphic units below the Lycian Allochthon (see Bozkurt & Oberhänsli (2001) for summary). A number of workers claim that the Menderes Massif was deformed, metamorphosed to amphibolite facies and intruded by granitoid magmas mainly during Tertiary burial below the Lycian Allochthon (Şengör *et al*. 1984; Erdoğan 1992; Bozkurt *et al*. 1993, 2001). On the basis of this suggested Alpine event, it has

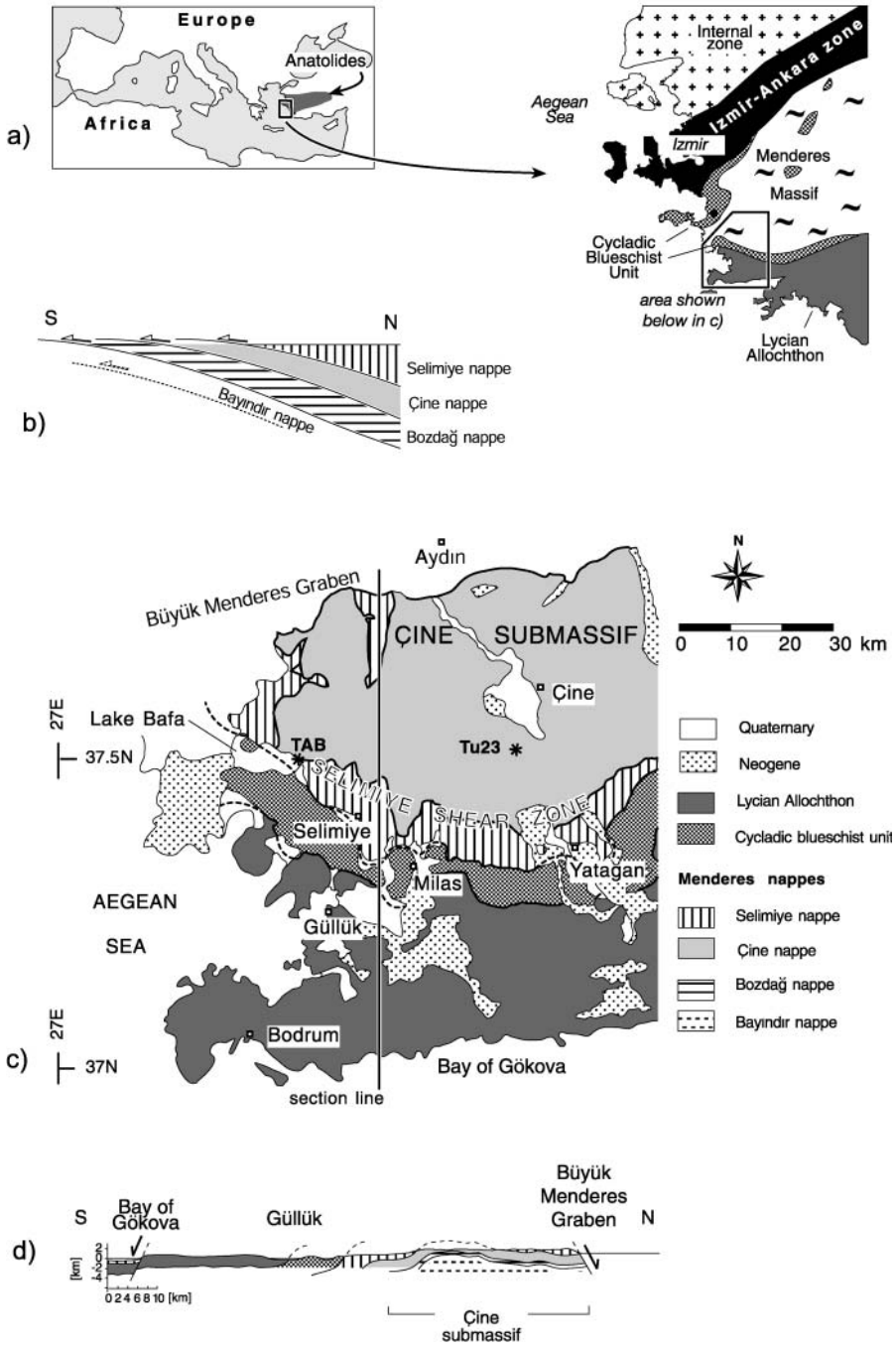

Fig. 1. Location and tectonic setting of study area (**a**). Tectonic units of the Menderes Massif in schematic profile (**b**; after Gessner *et al*. 2001*c*), simplified geological map (**c**), and cross-section (**d**). Sample localities are marked with asterisks. It should be noted that the Cycladic blueschist unit (in (**a**) and (**c**)) and the Izmir Ankara suture zone (in (**a**)) are shown for reference purposes only and are not discussed in the text. The implications of the general architecture for Alpine convergence have been discussed by Gessner *et al*. (2001*c*).

been argued that deformation fabrics associated with amphibolite-facies metamorphism in the basal units indicate north-directed tectonic transport during Tertiary convergence (Bozkurt *et al*. 1993; Lips *et al*. 2001; Özer & Sözbilir 2003). A series of studies, however, have questioned this hypothesis and claim that the apparently uniform north–south-trending structural grain across the belt may be the result of the superposition of Pan-African, and several stages of Alpine deformation fabrics (Hetzel *et al*. 1995; Gessner *et al*. 2001*a*, 2001*b*, 2001*c*; Ring *et al*. 2001).

Much controversy centres on the age of top-to-the-NNE kinematic indicators such as S–C fabrics, asymmetric feldspar porphyroclasts and shear bands, which are present in amphibolite-facies metamorphic rocks across the Menderes Massif. These fabrics are particularly prominent in granitoid rocks, which are characterized by a pervasive protomylonitic to mylonitic foliation (Bozkurt & Park 1997; Hetzel *et al*. 1998; Gessner *et al*. 2001*a*). A number of studies have inferred a Tertiary age for the intrusion of these granitoids into high-grade schists and gneisses, on the basis of an assumed stratigraphic continuity with fossil-bearing Palaeozoic and Mesozoic units, which occur along strike and up-section relative to the intruded rocks (Erdoğan 1992; Bozkurt *et al*. 1993). Contrary to this view, Gessner *et al*. (2001*a*, 2001*c*) argued that a distinct amphibolite-facies fabric S_{PA}, by and large associated with, but not limited to top-to-the-NNE kinematic indicators, is confined to certain tectonic slices (the Selimiye,

Çine and Bozdağ nappes, Fig. 2). According to those workers, an older group of granitoid rocks in the Çine and Selimiye nappes along with their wall rocks display S_{PA}, whereas later granitoid rocks intrude this fabric. Preliminary Pb/Pb zircon evaporation dating of the crosscutting granite yielded an age of 547.2 ± 1.0 Ma, which led Gessner *et al*. (2001*a*) to suggest that S_{PA} had formed in the Neoproterozoic or Cambrian. Because S_{PA} is also absent from Triassic granites in the Bozdağ nappe, Gessner *et al*. (2001*a*, 2001*c*) further argued that the final assembly of the nappe stack occurred during the Tertiary, when the amphibolite-facies fabrics were overprinted by a greenschist-facies fabric S_{A3} associated with top-to-the-south kinematic indicators. An alternative interpretation of the greenschist-facies top-to-the-south fabrics is that they represent late Alpine extension along the southern margin of the Çine submassif (Bozkurt *et al*. 1993; Whitney & Bozkurt 2002). This controversy is difficult to resolve from the structural and geochronological data available. Ductile fabrics and tectonic boundaries in the southern part of the Çine massif outline a large-scale monocline, the tectonic significance of which is not known. As there is no knowledge on the original orientation of the greenschist-facies shear zones in this region relative to the Earth's surface, their present south-dipping orientation cannot be used to infer crustal extension. It is clear, however, that the greenschist-facies fabrics are retrogressing an older, amphibolite-facies fabric along the Selimiye shear zone (Régnier *et al*. 2003).

An attempt at directly dating a greenschist-facies top-to-the-north fabric in a different tectonic unit was carried out by Lips *et al*. (2001), who dated white mica from mica schists in the Bayındır nappe (Fig. 1) and obtained an $^{40}Ar/^{39}Ar$ age of 36 ± 2 Ma. However, as Lips *et al*. (2001) pointed out, it is uncertain whether this age dates the fabric-forming event or cooling after a later thermal event, as the temperature history of the rock is poorly constrained. In addition to this uncertainty, the significance of this age in relation to kinematics is also questionable, as Gessner *et al*. (2001*b*) have reported that the Bayındır nappe is characterized by a pervasive asymmetric shear band foliation indicating top-to-the-south directed shearing across its entire range of outcrop (Fig. 2).

These contradicting interpretations demonstrate the need for age data to constrain the history of deformation, metamorphism and igneous activity in the Menderes Massif and to reconstruct the geodynamic history of this part of the Alpine chain.

Granitoid rocks and their ages

Pre-Miocene igneous rocks occur only in the lower tectonic units of the Menderes Massif; the Menderes nappes *sensu* Ring *et al*. (1999). According to those workers four tectonic units make up the Menderes nappes. The three structurally highest units, which are, from top to bottom, the Selimiye, the Çine and the Bozdağ nappes (Fig. 2), have been intruded by granitic magmas (Gessner *et al*. 2001*a*), the Bozdağ nappe apparently only by Triassic granites (Dannat 1997; Koralay *et al*. 2001). The occurrence of

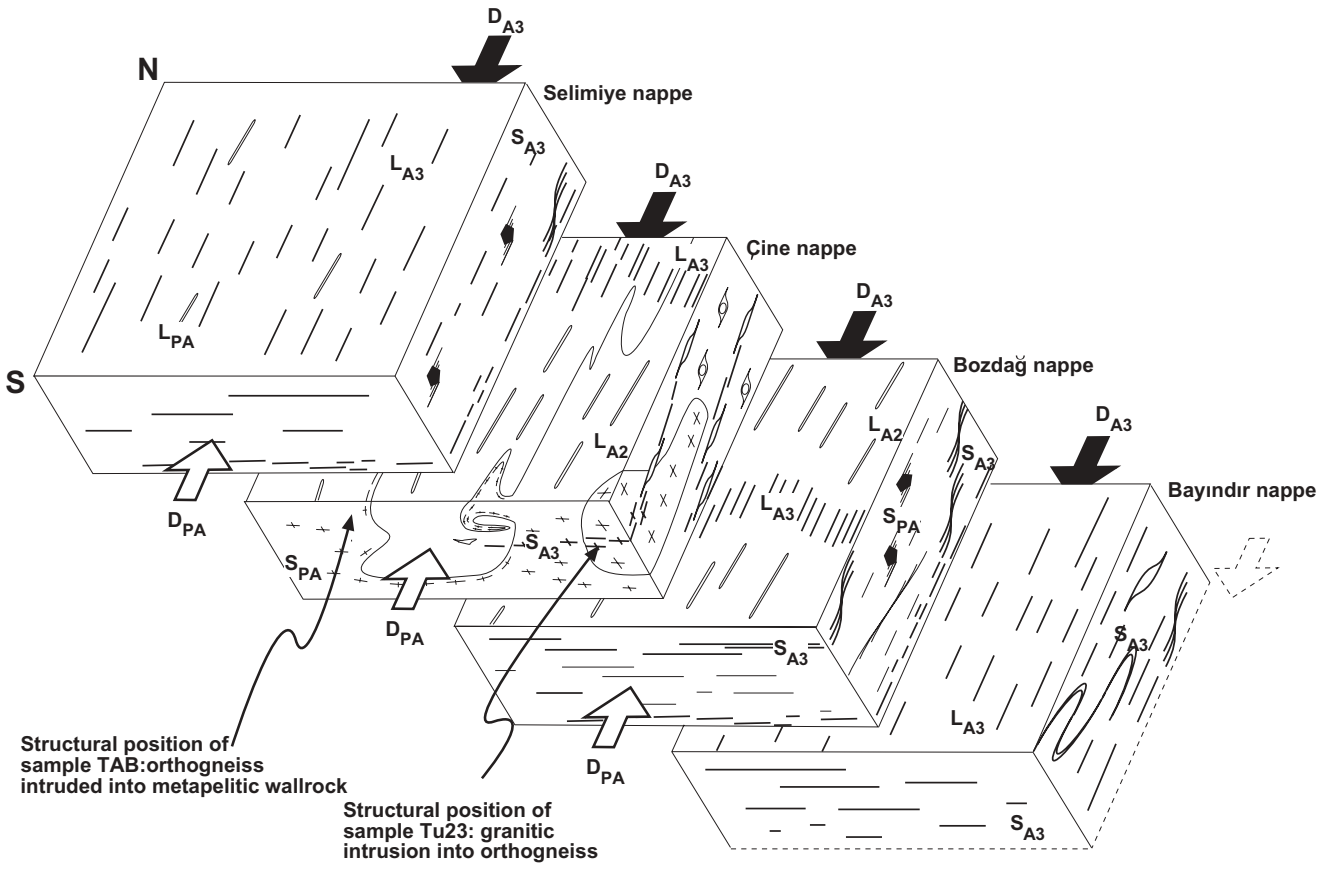

Fig. 2. Schematic diagram of Alpine age structures (lineation L_{A3}, foliation S_{A3}) associated with deformation event D_{A3} and their kinematics (arrows depict hanging-wall transport direction), which overprint pre-Alpine structures of D_{PA} in the Selimiye, Çine and Bozdağ nappe and are the only fabric in the Bayındır nappe.

Proterozoic to Cambrian basement including relicts of eclogite- and granulite-facies rock is also confined to these three units (Candan *et al*. 2001; Ring *et al*. 2001).

Granitoid rocks of the Çine nappe dominate the Çine submassif (Fig. 1c), the southern margin of which is highly sheared and forms the greenschist-facies top-to-the-south Selimiye shear zone (Ring *et al*. 1999; Fig. 1c). In a few places (e.g. at the north shore of Bafa Lake, Fig. 1c) an intrusive relationship occurs between granitoid rocks and schists, which have been correlated with Palaeozoic and Mesozoic metapelites and marbles elsewhere in the Menderes Massif (Erdoğan 1992; Bozkurt *et al*. 1993). This correlation, however, is ill supported by the available geochronological data, which suggest that the granites along the granite–schist contact, and in a large number of other locations across the Menderes Massif, crystallized in Neoproterozoic and Cambrian times (e.g. Hetzel & Reischmann 1996; Dannat 1997; Hetzel *et al*. 1998; Loos & Reischmann 1999; Gessner *et al*. 2001*a*). On the basis of the discrepancy between stratigraphic correlation and isotopic age data, Bozkurt *et al*. (2001) suggested that the zircon ages were likely to be inherited protolith ages and argued in favour of Alpine granitoid intrusions.

The metapelitic and metacarbonaceous Bayındır nappe (after Ring *et al*. 1999) constitutes the lowest, possibly a para-autochthonous tectonic unit of the Menderes Massif, with protolith ages ranging from Permo-Carboniferous (Okay 2001) to Cretaceous (Özer & Sözbilir 2003). Apart from a small, enigmatic granite in the southeastern Ödemis submassif (O. Candan, pers. comm.) and post-contractional Miocene granitoids in the central part of the Menderes Massif (Hetzel *et al*. 1995), no intrusions have been reported in the Bayındır nappe.

Samples and methods

The samples were chosen from two outcrops of the Çine submassif and represent key relations between age and deformation history of the granitoid rocks in the Menderes Massif. Sample Tu23 comes from an outcrop 2.4 km along the road from Akçaova to Eskiçine that had also been sampled for single-zircon evaporation dating by Gessner *et al*. (2001*a*). The outcrop is characterized by intrusion of an undeformed granite into the amphibolite-facies fabric of a top-to-the-north sheared orthogneiss. Dating the intrusion age of the former thus constrains the minimum age of the regional-scale amphibolite-facies top-to-the-north shearing.

Sample TAB is from one of the granites that intruded into amphibolite-facies mica schist at the northeastern end of Lake Bafa (37°29.702′N, 27°32.417′E). Undeformed portions of this intrusion can be traced into ductile deformed intrusive contacts, which are folded by two generations of folds with axes oriented parallel to each other, and parallel to the steeply south-plunging stretching lineation within the Selimiye shear zone. Dating the rims of magmatic zircons in this sample constrains the latest crystallization age of the granite and provides a minimum age of the mica schist unit along the Selimiye shear zone.

Heavy minerals were separated from the samples by heavy liquid and magnetic techniques. Zircons were hand picked, mounted in epoxy resin, polished, cleaned and gold coated. Cathodoluminescence (CL) imaging was carried out to characterize the zircons and identify areas for analysis. Luminescence images were also used to identify and distinguish core from rims, and we use this textural distinction throughout this paper.

U–Pb isotopic data were collected by SIMS on the SHRIMP II of the John de Laeter Centre of Mass Spectrometry, Perth. Sensitivity for Pb isotopes in zircon was *c*. 18 c.p.s. ppm^{-1} per nA, primary beam current was 2.5–3.0 nA and mass resolution was *c*. 5000. Correction of measured isotopic ratios for common Pb was based on the measured ^{204}Pb in each sample and usually represented a <1% correction to the ^{206}Pb counts (see % common ^{206}Pb in Tables 1 and 2). The common Pb component, being small and largely a surface contaminant, was modelled on the composition of Broken Hill Pb ore. Seven mass scans were undertaken on each analysis to enhance precision. Pb/U isotopic ratios were corrected for instrumental inter-element discrimination using the observed covariation between Pb^+/U^+ and UO^+/U^+ (Compagnoni *et al*. 1977; Compston *et al*. 1984, 1992, 1995) determined from interspersed analyses of the Perth standard zircon CZ3. CZ3 is a single zircon megacryst from Sri Lanka with an age of 564 Ma and a ^{206}Pb/^{238}U value of 0.0914 (Nelson 1997).

SHRIMP U–Pb zircon results

Zircons from sample TAB form two main populations based on morphology and luminescence textures. The first population consists of squat pyramidal crystals that commonly contain distinct cores. The second population are prismatic zircons of large aspect ratio (*c*. 3.5:1 to 5:1) without any distinguishable cores. In CL images the cores are commonly dark and show evidence of resorption whereas the rims luminesce more readily and are oscillatory zoned. The long prismatic crystals preserve oscillatory zoning that is commonly modified by irregular, highly luminescent zircon. The cores of the squat grains range in age from 1929 ± 26 Ma to 568 ± 15 Ma (Fig. 3a). These grains are interpreted as xenocrysts, as many are partially resorbed and their CL patterns are truncated by younger rims. The youngest core analysis is of identical age to the interpreted magmatic age (see below) and may have recrystallized in the magma. A number of analyses (17) produced <10% discordant ^{206}Pb/^{238}U ages between 500 and 600 Ma (Fig. 3a). These combine to produce a weighted mean age of 552 ± 11 Ma (95% confidence, $n = 17$, MSWD = 2.4). Ten of these analyses were of concordant zircon rims and long prismatic grains that also spanned a similar age range, with ^{206}Pb/^{238}U ages between 512 ± 13 Ma and 570 ± 15 Ma. A weighted mean age of 541 ± 14 Ma (95% confidence, $n = 10$, MSWD = 1.9, Fig. 3) was obtained from these zircons with luminescent textures consistent with magmatic growth, and this age is interpreted as the most accurate representation of the crystallization age of the granite.

U–Pb analyses were obtained from 32 analytical sites in sample Tu23 (Fig. 3b). CL images clearly identify two contrasting zircon populations similar to sample TAB, with cores and highly luminescent rims in squat pyramidal grains, and large aspect ratio coreless prismatic crystals (Fig. 3b). Core analyses yielded ^{206}Pb/^{238}U ages of between *c*. 560 and 840 Ma. The younger of these analyses give ages identical to the interpreted age of magmatism (see below) and these zircons either crystallized in the magma or were isotopically reset at this time. Twenty analyses of rims and prismatic grains were used to produce a σ weighted mean age of 564.0 ± 7 Ma (95% confidence, $n = 20$, MSWD = 0.60). Many of these analyses were slightly negatively discordant, which may be a result of imprecise common Pb modelling. However, when only the <10% discordant analyses are averaged, a very similar result is obtained (566 ± 9 Ma, 95% confidence, $n = 14$, MSWD = 0.36). We interpret 566 ± 9 Ma as the most accurate representation of the crystallization age of the granitic protolith.

Similar basement provinces in the Eastern Mediterranean

The Menderes Massif is part of the Menderes–Tauride Block (Robertson & Dixon 1984; Robertson *et al*. 1996), a post-Permian microcontinent, which is allochthonous with respect to both Eurasia and Gondwana. Most reconstructions place the

Table 1. *U and Pb isotope and elemental abundance (U and Th) data for sample TAB*

Spot	Type	U (ppm)	Th (ppm)	$^{232}Th/^{238}U$	% common ^{206}Pb	$^{206}Pb^*/^{238}U$	±†	$^{207}Pb^*/^{235}U$	±†	$^{207}Pb^*/^{206}Pb$	±†	$^{206}Pb^*/^{238}U$ age	±†	$^{207}Pb^*/^{206}Pb$ age	±†	% discordant
TAB.01	lp	229	70	0.31	−0.04	0.0895	0.0024	0.72	0.02	0.0582	0.0008	552	15	537	30	−3
TAB.02	lp	231	66	0.29	0.19	0.0917	0.0025	0.71	0.02	0.0560	0.0009	567	15	454	37	−25
TAB.03	r	620	50	0.08	0.07	0.0927	0.0025	0.74	0.02	0.0577	0.0005	572	15	519	21	−10
TAB.04	c	495	805	1.68	0.01	0.1041	0.0028	0.87	0.02	0.0604	0.0005	646	22	619	18	−3
TAB.05	r	433	16	0.04	−0.12	0.0923	0.0025	0.75	0.02	0.0593	0.0007	569	15	577	27	1
TAB.06	c	413	41	0.10	0.26	0.0894	0.0024	0.70	0.02	0.0565	0.0008	554	14	470	31	−17
TAB.07	c	122	41	0.35	0.01	0.3588	0.0116	5.85	0.21	0.1182	0.0017	1981	58	1929	26	−2
TAB.08	r	268	47	0.18	0.43	0.1026	0.0028	0.91	0.04	0.0644	0.0020	629	17	756	65	17
TAB.09	c	528	60	0.12	0.05	0.0920	0.0025	0.74	0.02	0.0586	0.0005	567	15	553	20	−3
TAB.10	c	434	38	0.09	−0.03	0.0921	0.0025	0.75	0.02	0.0588	0.0005	568	15	558	20	−2
TAB.11	c	184	215	1.21	−0.05	0.0937	0.0026	0.79	0.02	0.0609	0.0009	575	19	636	31	9
TAB.12	r	286	67	0.24	−0.01	0.0925	0.0025	0.75	0.02	0.0586	0.0007	569	15	550	25	−4
TAB.13	lp	356	46	0.13	−0.01	0.0913	0.0025	0.74	0.02	0.0585	0.0006	563	15	549	22	−3
TAB.14	lp	168	45	0.28	−0.04	0.0910	0.0025	0.73	0.02	0.0583	0.0009	561	15	541	35	−4
TAB.15	c	505	50	0.10	0.13	0.0892	0.0024	0.71	0.02	0.0575	0.0007	551	14	510	26	−8
TAB.16	r	182	41	0.23	0.30	0.0860	0.0024	0.70	0.03	0.0593	0.0020	531	14	577	72	8
TAB.17	lp	500	272	0.56	0.15	0.0827	0.0022	0.64	0.02	0.0565	0.0006	513	15	471	24	−9
TAB.18	c	484	86	0.18	0.10	0.0873	0.0024	0.68	0.02	0.0569	0.0005	540	15	487	20	−11
TAB.19	c	356	73	0.21	0.10	0.1859	0.0056	2.39	0.07	0.0933	0.0007	1094	31	1494	15	26
TAB.20	lp	240	57	0.25	0.32	0.0829	0.0022	0.63	0.02	0.0550	0.0011	516	14	412	45	−25
TAB.21	c	969	43	0.05	1.16	0.0743	0.0021	0.59	0.03	0.0578	0.0022	461	13	522	82	12
TAB.22	c	404	360	0.92	0.07	0.0973	0.0027	0.79	0.02	0.0589	0.0006	599	18	563	23	−6
TAB.23	r	460	27	0.06	0.13	0.0846	0.0023	0.67	0.02	0.0571	0.0006	524	14	495	24	−6
TAB.24	c	38	10	0.27	−0.06	0.0976	0.0029	0.82	0.03	0.0611	0.0014	599	18	644	48	7
TAB.25	c	344	55	0.17	0.17	0.0955	0.0026	0.76	0.02	0.0575	0.0006	590	16	511	24	−15
TAB.26	c	1704	524	0.32	0.02	0.1171	0.0031	1.01	0.03	0.0627	0.0003	711	19	698	9	−2
TAB.27	r	491	52	0.11	0.13	0.0886	0.0024	0.70	0.02	0.0571	0.0004	548	14	497	17	−10
TAB.28	lp	211	41	0.20	0.03	0.0855	0.0027	0.69	0.02	0.0585	0.0006	528	16	548	23	3
TAB.29	lp	389	38	0.10	0.17	0.0881	0.0024	0.70	0.02	0.0578	0.0005	545	14	523	20	−4
TAB.30	c	340	195	0.59	0.26	0.0857	0.0023	0.70	0.02	0.0589	0.0011	528	15	565	42	6
TAB.31	r	248	74	0.31	−0.10	0.0818	0.0022	0.67	0.02	0.0594	0.0006	503	14	581	21	13
TAB.32	c	544	57	0.11	0.14	0.0886	0.0024	0.69	0.02	0.0565	0.0006	548	15	473	23	−16
TAB.33	c	261	52	0.21	0.27	0.0889	0.0024	0.68	0.02	0.0559	0.0010	551	15	449	41	−22
TAB.34	lp	353	274	0.80	0.22	0.0871	0.0023	0.67	0.02	0.0561	0.0008	538	16	455	32	−18

C, core; r, rim; lp, long prismatic (see text for explanation).
*Radiogenic Pb only.
†All errors are absolute, 1σ errors.

Table 2. *U and Pb isotope and elemental abundance (U and Th) data for sample Tu23*

Spot	Type	U (ppm)	Th (ppm)	$^{232}Th/^{238}U$	% common ^{206}Pb	$^{206}Pb^*/^{238}U$	±†	$^{207}Pb^*/^{235}U$	±†	$^{207}Pb^*/^{206}Pb$	±†	$^{206}Pb^*/^{238}U$ age	±†	$^{207}Pb^*/^{206}Pb$ age	±†	% discordant
Tu23.01	lp	127	101	0.83	0.31	0.0909	2.2	0.75	4.0	0.0600	3.3	561	12	604	72	7
Tu23.02	r	263	38	0.15	0.59	0.0876	2.1	0.66	3.7	0.0543	3.0	541	11	384	68	−41
Tu23.03	r	516	61	0.12	0.34	0.0913	1.9	0.71	2.6	0.0565	1.8	563	10	474	40	−19
Tu23.04	c	449	538	1.24	0.37	0.1076	1.9	0.90	3.2	0.0606	2.6	659	12	626	55	−5
Tu23.05	r	349	35	0.10	0.25	0.0936	1.9	0.75	2.7	0.0579	1.9	577	11	525	41	−10
Tu23.06	r	527	63	0.12	0.08	0.0915	3.3	0.73	3.6	0.0581	1.5	565	18	532	32	−6
Tu23.07	c	316	63	0.21	0.35	0.0922	3.4	0.72	3.9	0.0565	2.0	569	18	471	45	−17
Tu23.08	c	235	27	0.12	0.42	0.0951	3.4	0.75	4.4	0.0569	2.8	586	19	488	62	−17
Tu23.09	c	497	44	0.09	0.15	0.0949	3.4	0.77	3.6	0.0588	1.2	585	19	558	26	−4
Tu23.10	r	669	55	0.09	0.02	0.0963	3.3	0.79	3.5	0.0593	1.1	593	19	576	23	−3
Tu23.11	c	202	85	0.43	0.45	0.1345	3.7	1.17	4.4	0.0631	2.4	813	28	710	51	−13
Tu23.12	r	286	28	0.10	0.35	0.0945	3.4	0.74	4.4	0.0566	2.8	582	19	476	62	−18
Tu23.13	lp	388	226	0.60	0.40	0.0915	3.3	0.76	4.0	0.0601	2.2	565	18	607	47	7
Tu23.14	r	398	51	0.13	0.16	0.0910	3.3	0.73	3.7	0.0585	1.5	561	18	548	32	−2
Tu23.15	c	562	63	0.12	0.21	0.0937	3.3	0.74	3.7	0.0569	1.6	578	18	489	36	−15
Tu23.16	r	428	61	0.15	0.26	0.0892	3.3	0.70	3.6	0.0566	1.3	551	18	477	29	−13
Tu23.17	r	267	39	0.15	0.41	0.0897	3.4	0.71	4.1	0.0571	2.3	554	18	496	51	−10
Tu23.18	c	602	244	0.42	0.58	0.1103	3.4	0.89	3.9	0.0587	2.0	674	22	557	44	−17
Tu23.19	lp	376	62	0.17	0.32	0.0894	3.3	0.71	3.8	0.0574	1.8	552	18	507	39	−8
Tu23.20	c	578	34	0.06	0.15	0.0929	3.4	0.77	3.5	0.0604	1.1	573	18	619	23	8
Tu23.21	r	2123	114	0.06	0.02	0.0927	3.3	0.75	3.4	0.0586	0.5	571	18	554	10	−3
Tu23.22	c	282	51	0.19	0.02	0.1064	3.4	0.91	3.8	0.0620	1.7	652	21	676	36	4
Tu23.23	c	574	56	0.10	0.31	0.0905	3.4	0.71	3.8	0.0571	1.7	558	18	496	37	−11
Tu23.24	c	349	41	0.12	0.16	0.0941	3.3	0.75	3.8	0.0576	1.8	580	19	516	39	−11
Tu23.25	r	316	28	0.09	0.16	0.0941	3.4	0.75	3.8	0.0576	1.8	580	19	514	38	−11
Tu23.26	r	282	37	0.14	0.08	0.0916	3.4	0.76	3.9	0.0604	1.9	565	19	617	41	9
Tu23.27	r	739	59	0.08	0.01	0.0916	3.4	0.74	3.7	0.0587	1.4	565	18	557	30	−1
Tu23.28	c	177	66	0.39	2.30	0.1035	4.4	0.90	8.2	0.0629	7.0	635	27	706	148	11
Tu23.29	r	377	73	0.20	0.07	0.0917	3.4	0.74	3.7	0.0589	1.5	565	18	562	32	−1
Tu23.30	r	305	30	0.10	0.30	0.0920	3.4	0.73	4.1	0.0575	2.4	568	18	510	52	−10
Tu23.31	r	514	50	0.10	0.13	0.0907	3.3	0.73	3.5	0.0580	1.1	559	18	530	24	−5
Tu23.32	r	831	66	0.08	0.22	0.0911	3.3	0.71	3.5	0.0567	1.2	562	18	478	26	−15

C, core; r, rim; lp, long prismatic (see text for explanation).
*Radiogenic Pb only.
†All errors are absolute, 1σ errors.

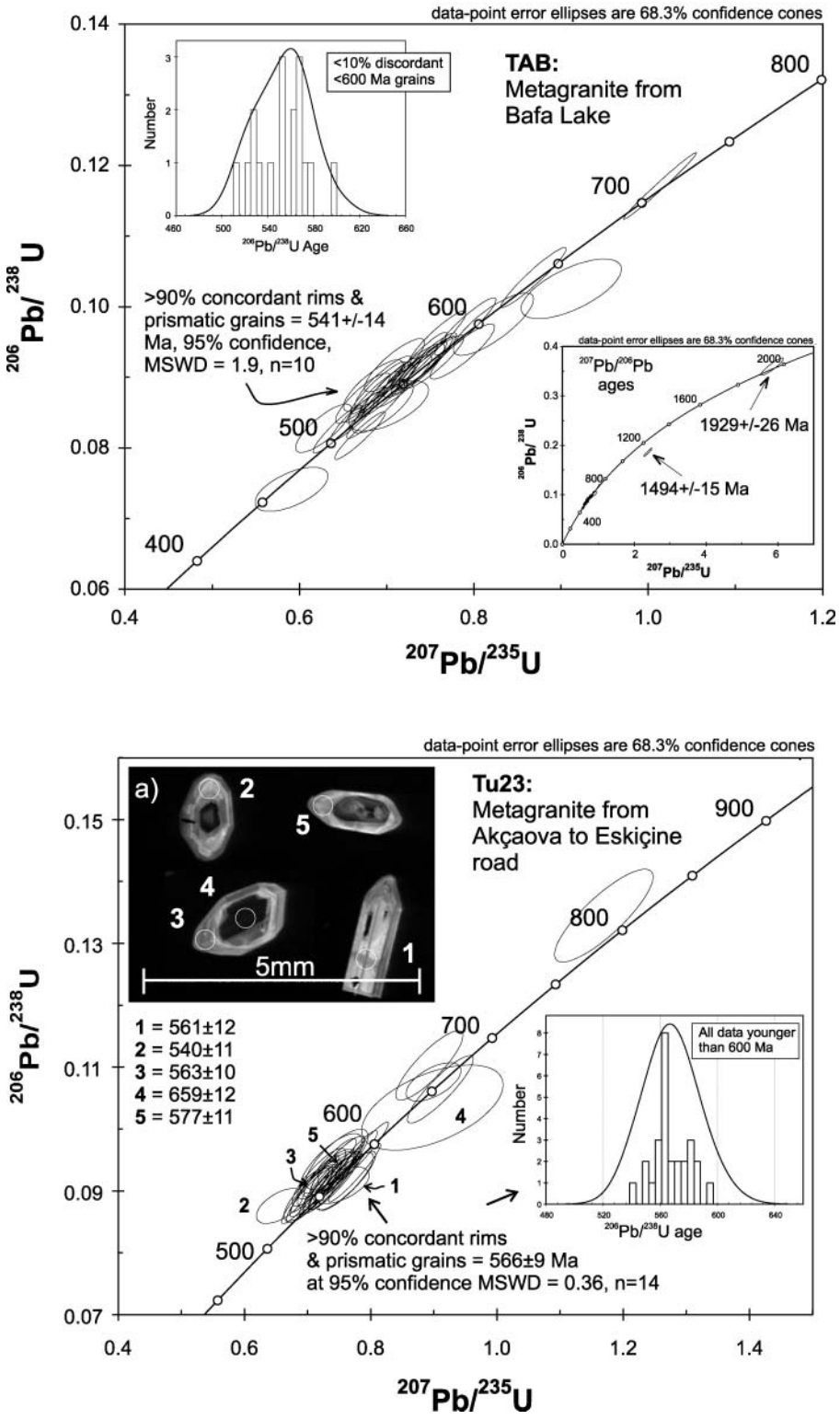

Fig. 3. Concordia diagrams and statistics of SHRIMP U–Pb isotopic measurements from sample TAB (**a**) and Tu23 (**b**); inset in (**b**) shows CL images of analysis points in homogeneous long-prismatic (1) and zoned pyramidal (2–5) zircon grains.

Menderes–Tauride Block adjacent to Egypt and the Levant (Robertson *et al*. 1996; Stampfli & Borel 2002). The closest exposed basement rocks occur in Egypt's North Eastern Desert, where igneous activity has been reported from 611 to 563 Ma (at maximum uncertainty) (Stern & Hedge 1985; Sultan *et al*. 1990; Wilde & Youssef 2000). In the Central Eastern Desert a 779 ± 4 Ma orthogneiss contains amphibolite xenoliths yielding an age of 1149 Ma (Loizenbauer *et al*. 2001), whereas throughout the Eastern Desert the metasedimentary Hammamat Group contains numerous detrital zircons dated between 600 and 800 Ma with a number of older grains that date back to the Archaean (Wilde & Youssef 2002).

Significance of the ages to the structural history

U–Pb ages measured for magmatic zircons in the southern Menderes Massif are Neoproterozoic to earliest Cambrian, with the youngest ages occurring in homogeneous long-prismatic crystals and rims of pyramidal grains with inherited cores. The xenocrysts provide evidence that earlier Neoproterozoic rocks were present in the region and that locally rocks date back to 1929 Ma. These data support a pre-Mesozoic location of the Menderes–Tauride Block adjacent to northern Egypt, where rocks in the North Eastern and Central Eastern Desert have age distributions similar to the Menderes Massif rocks analysed in this study.

With regard to the Alpine Orogeny, the results support geochronological studies that propose a pre-Alpine age of magmatism, high-grade metamorphism and amphibolite-facies deformation fabrics for basement units of the Menderes Massif (Ring *et al*. 1999, 2001; Gessner *et al*. 2001*a*, 2001*c*). It has been repeatedly suggested that the metamorphic history of basement rocks in the southern Menderes Massif is one of a single event (Ashworth & Evirgen 1986; Whitney & Bozkurt 2002). In the light of recent geochronological, structural and metamorphic investigations, there is no compelling evidence for an orogenic-scale thermal event related to Alpine convergence, as suggested by Şengör *et al*. (1984), and re-invoked by a number of studies since (i.e.Ashworth & Evirgen 1984; Bozkurt *et al*. 1993; Whitney & Bozkurt 2002). It appears more likely that Alpine crustal shortening is solely recorded in retrograde south-displacing greenschist-facies shear zones, which have been shown to overprint earlier structures (Gessner *et al*. 2001*c*) and metamorphic assemblages (Régnier *et al*. 2003).

Conclusion

Combining the U–Pb SIMS technique with detailed structural analysis constrains the thermal and structural history of the polyorogenic and structurally complex Menderes Massif. Neoproterozoic to Cambrian U–Pb ages of magmatic zircons indicate that the granites of the Çine submassif and top-to-the-NNE kinematic indicators in these rocks formed at Neoproterozoic to Cambrian times. For key outcrops in the Çine submassif no evidence has been found for any Tertiary igneous activity. At the time of magmatism these basement rocks were possibly continuous with, or located close to Gondwana's northern margin. The Neoproterozoic to Cambrian age of amphibolite-facies metamorphisms and related deformation fabric development implies that the Alpine tectonic evolution of basement rocks in the southern Menderes Massif is confined to greenschist-facies shear zones with top-to-the-south kinematic indicators.

K.G. has been supported by a scholarship of the German Academic Exchange Service DAAD (Gemeinsames Hochschulsonderprogramm III von Bund und Ländern). A.S.C. thanks the ARC-funded Tectonics SRC and St Francis Xavier University, Nova Scotia, for providing facilities to complete this study. His contribution forms TSRC publication 229. A. Kennedy, P. Kinny and A. Nemchin are thanked for help using the SHRIMP. R. Sliwa, Y. Zhang, P. Alt-Epping and R. England are thanked for comments. Constructive reviews by A.H.F. Robertson and P. Hoskin significantly improved the manuscript.

References

Ashworth, J.R. & Evirgen, M.M. 1984. Garnet and associated minerals in the southern margin of the Menderes Massif, southwest Turkey. *Geological Magazine*, **121**, 323–337.

Bozkurt, E. & Oberhänsli, R. 2001. Menderes Massif (western Turkey): structural, metamorphic and magmatic evolution—a synthesis. *International Journal of Earth Sciences*, **89**, 679–708.

Bozkurt, E. & Park, R.G. 1997. Microstructures of deformed grains in the augen gneisses of southern Menderes Massif (western Turkey) and their tectonic significance. *Geologische Rundschau*, **86**, 103–119.

Bozkurt, E., Park, R.G. & Winchester, J.A. 1993. Evidence against the core/cover interpretation of the southern sector of the Menderes massif, west Turkey. *Terra Nova*, **5**, 445–451.

Bozkurt, E., Park, R.G., Loos, S. & Reischmann, T. 2001. Discussion on the evolution of the Southern Menderes Massif in SW Turkey as revealed by zircon dating. *Journal of the Geological Society, London*, **158**, 393–395.

Candan, O., Dora, O.Ö., Oberhänsli, R., Çetinkaplan, M., Partzsch, J.H., Warkus, F.C. & Dürr, S. 2001. Pan-African high-pressure metamorphism in the Precambrian basement of the Menderes Massif, western Anatolia, Turkey. *International Journal of Earth Sciences*, **89**, 793–811.

Collins, A.S. & Robertson, A.H.F. 1997. Lycian melange, southwestern Turkey: an emplaced Late Cretaceous accretionary complex. *Geology*, **25**, 255–258.

Collins, A.S. & Robertson, A.H.F. 1998. Processes of Late Cretaceous to Late Miocene episodic thrust-sheet translation in the Lycian Taurides, SW Turkey. *Journal of the Geological Society, London*, **155**, 759–772.

Collins, A.S. & Robertson, A.H.F. 1999. Evolution of the Lycian Allochthon, western Turkey, as a north-facing Late Palaeozoic–Mesozoic rift and passive continental margin. *Geological Journal*, **34**, 107–138.

Collins, A.S. & Robertson, A.H.F. 2003. Kinematic evidence for Late Mesozoic–Miocene emplacement of the Lycian Allochthon over the western Anatolide belt, SW Turkey. *Geological Journal*, **xx**, xx–xxx.

Compagnoni, R., Dal Piaz, G.V., Hunziker, J.C., Gosso, G., Lombardo, B. & Williams, P.F. G.V., Hunziker, J.C., Gosso, G., Lombardo, B. & Williams, P.F. 1977. The Sesia–Lanzo Zone, a slice of continental crust with Alpine high pressure–low temperature assemblages in the western Italian Alps. *Rendiconti della Società Italiana di Mineralogia e Petrologia*, **33**, 281–334.

Compston, W., Williams, I.S. & Meyer, C. 1984. U–Pb geochronology of zircons from lunar breccia 73217 using a sensitive high mass-resolution ion microprobe. *Journal of Geophysical Research*, **89**(Supplement), B525–B534.

Compston, W., Williams, I.S., Kirschvink, J.L., Zhang, Z. & Ma, G. 1992. Zircon U–Pb ages for the Early Cambrian time scale. *Journal of the Geological Society, London*, **149**, 171–184.

Compston, W., Sambridge, M.S., Reinfrank, R.F., Moczydlowska, M., Vidal, G. & Claesson, S. 1995. Numerical ages of volcanic rocks and the earliest faunal zone within the Late Precambrian of east Poland. *Journal of the Geological Society, London*, **152**, 599–611.

Dannat, C. 1997. *Geochemistry, geochronology and Nd–Sr isotopy of granitoid core gneisses of the Menderes Massif, southwest Turkey*. PhD thesis, Johannes Gutenberg University, Mainz.

De Graciansky, P.-C. 1972. *Recherches géologiques dans le Taurus Lycien Occidental*. DSc thesis, University of Paris.

Erdoğan, B. 1992. Problem of core–mantle boundary of Menderes Massif. *In:* Anil, M. & Nazik, N. (eds) *Proceedings of the International Symposium on Eastern Mediterranean Geology, Adana. Geosound*, 314–315.

Gessner, K., Piazolo, S., Güngör, T., Ring, U., Kröner, A. & Passchier, C.W. 2001a. Tectonic significance of deformation patterns in granitoid rocks of the Menderes nappes, Anatolide belt, southwest Turkey. *International Journal of Earth Sciences*, **89**, 766–780.

Gessner, K., Ring, U., Johnson, C., Hetzel, R., Passchier, C. & Güngör, T. 2001b. An active bivergent rolling-hinge detachment system: Central Menderes Metamorphic Core Complex in western Turkey. *Geology*, **29**, 611–614.

Gessner, K., Ring, U., Passchier, C.W. & Güngör, T. 2001c. How to resist subduction: evidence for large-scale out-of-sequence thrusting during Eocene collision in western Turkey. *Journal of the Geological Society, London*, **158**, 769–784.

Hetzel, R. & Reischmann, T. 1996. Intrusion age of Pan-African augen gneisses in the southern Menderes Massif and the age of cooling after Alpine ductile extensional deformation. *Geological Magazine*, **133**, 565–572.

Hetzel, R., Passchier, C.W., Ring, U. & Dora, O.Ö. 1995. Bivergent extension in orogenic belts: the Menderes massif (southwestern Turkey). *Geology*, **23**, 455–458.

Hetzel, R., Romer, R.L., Candan, O. & Passchier, C.W. 1998. Geology of the Bozdag area, central Menderes massif, SW Turkey: Pan-African basement and Alpine deformation. *Geologische Rundschau*, **87**, 394–406.

Koralay, O.E., Satir, M. & Dora, O.Ö. 2001. Geochemical and geochronological evidence for Early Triassic calc-alkaline magmatism in the Menderes Massif, western Turkey. *International Journal of Earth Sciences*, **89**, 822–835.

Lips, A.L.W., Cassard, D., Sözbilir, H., Yilmaz, H. & Wijbrans, J.R. 2001. Multistage exhumation of the Menderes Massif, western Anatolia. *International Journal of Earth Sciences*, **89**, 781–792.

Loizenbauer, J., Wallbrecher, E., Fritz, H., Neumayr, P., Khudeir, A.A. & Kloetzli, U. 2001. Structural geology, single zircon ages and fluid inclusion studies of the Meatiq metamorphic core complex; implications for Neoproterozoic tectonics in the Eastern Desert of Egypt. *Precambrian Research*, **110**, 357–383.

Loos, S. & Reischmann, T. 1999. The evolution of the southern Menderes Massif in SW Turkey as revealed by zircon dating. *Journal of the Geological Society, London*, **156**, 1021–1030.

Nelson, D.R. 1997. *Compilation of SHRIMP U–Pb Zircon Geochronology Data, 1996*. Geological Survey of Western Australia Record, **1997/2**.

Okay, A.I. 1989. Geology of the Menderes Massif and the Lycian Nappes south of Denizli, western Taurides. *Mineral Research Exploration Bulletin (Ankara)*, **109**, 37–51.

Okay, A.I. 2001. Stratigraphic and metamorphic inversions in the central Menderes Massif: a new structural model. *International Journal of Earth Sciences*, **89**, 709–727.

Özer, S. & Sözbilir, H. 2003. Presence and tectonic significance of Cretaceous rudist species in the so-called Permo-Carboniferous Göktepe Formation, central Menderes metamorphic massif, western Turkey. *International Journal of Earth Sciences*, DOI 10.1007/s00531-003-0333-z.

Paréjas, E. 1940. La tectonique transversale de la Turquie. *Reviews of the Faculty of Science of the University of Istanbul, Series B*, **5**, 133–244.

Régnier, J.-L., Ring, U., Passchier, C.W., Güngör, T. & Gessner, K. 2003. Contrasting metamorphic evolution of metasedimentary rocks from the Çine and Selimiye nappes in the Anatolide belt, western Turkey. *Journal of Metamorphic Geology*, **21**, 699–722.

Ring, U., Gessner, K., Güngör, T. & Passchier, C.W. 1999. The Menderes Massif of western Turkey and the Cycladic Massif in the Aegean—do they really correlate? *Journal of the Geological Society, London*, **156**, 3–6.

Ring, U., Willner, A.P. & Lackmann, W. 2001. Stacking of nappes with different pressure–temperature paths: an example from the Menderes nappes of western Turkey. *American Journal of Science*, **301**, 912–944.

Robertson, A.H. & Dixon, J.E. 1984. Aspects of the geological evolution of the eastern Mediterranean. *In:* Dixon, J.E. & Robertson, A.H.F. (eds) *The Geological Evolution of the Eastern Mediterranean*. Geological Society, London, Special Publications, **17**, 1–74.

Robertson, A.H.F., Dixon, J.E., Brown, S., Collins, A.S., Pickett, E., Sharp, I. & Ustaömer, T. 1996. Alternative tectonic models for the Late Palaeozoic–Early Tertiary development of Tethys in the Eastern Mediterranean region. *In:* Morris, A. & Tarling, D.H. (eds) *Palaeomagnetism and Tectonics of the Mediterranean Region*. Geological Society, London, Special Publications, **105**, 239–263.

Şengör, A.M.C. 1987. Cross-faults and differential stretching of hanging walls in regions of low-angle normal faulting; examples from western Turkey. *In:* Coward, M.P., Dewey, J.F. & Hancock, P.L. (eds) *Continental Extensional Tectonics*. Geological Society, London, Special Publications, **28**, 575–589.

Şengör, A.M.C. & Yilmaz, Y. 1981. Tethyan evolution of Turkey: a plate tectonic approach. *Tectonophysics*, **75**, 181–241.

Şengör, A.M.C., Satir, M. & Akkök, R. 1984. Timing of the tectonic events in the Menderes massif, western Turkey: implications for tectonic evolution and evidence for Pan-African basement in Turkey. *Tectonics*, **3**, 693–707.

Seyitoğlu, G., Scott, B. & Rundle, C.C. 1992. Timing of Cenozoic extensional tectonics in west Turkey. *Journal of the Geological Society, London*, **149**, 533–538.

Stampfli, G.M. & Borel, G.D. 2002. A plate tectonic model for the Paleozoic and Mesozoic constrained by dynamic plate boundaries and restored synthetic oceanic isochrons. *Earth and Planetary Science Letters*, **196**, 17–33.

Stern, R.J. & Hedge, C.E. 1985. Geochronologic and isotopic constraints on late Precambrian crustal evolution in the Eastern Desert of Egypt. *American Journal of Science*, **285**, 97–127.

Sultan, M., Chamberlain, K.R., Bowring, S.A., Arvidson, R.E., Abuzied, H. & El Kaliouby, B. 1990. Geochronologic and isotopic evidence for involvement of pre-Pan-African crust in the Nubian Shield, Egypt. *Geology*, **18**, 761–764.

Whitney, D.L. & Bozkurt, E. 2002. Metamorphic history of the southern Menderes Massif, western Turkey. *Geological Society of America Bulletin*, **114**, 829–838.

Wilde, S.A. & Youssef, K. 2000. Significance of SHRIMP U–Pb dating of the imperial porphyry and associated Dokhan Volcanics, Gebel Dokhan, North Eastern Desert, Egypt. *Journal of African Earth Sciences*, **31**, 403–413.

Wilde, S.A. & Youssef, K. 2002. A re-evaluation of the origin and setting of the Late Precambrian Hammamat Group based on SHRIMP U–Pb dating of detrital zircons from Gebel Umm Tawat, North Eastern Desert, Egypt. *Journal of the Geological Society, London*, **159**, 595–604.

Received 23 November 2002; revised typescript accepted 12 July 2003.
Scientific editing by Martin Whitehouse